**Military Technical College**
Kobry El-Kobbah,
**Cairo, Egypt**

**8th International Conferenc**
**on**
**Chemical & Environmenta**
**Engineering**
19 – 21 April 2016

**TANM -3**

# Facile Synthesis of Nano-Magnetic Ferberite -Graphene for Uranium Adsorption

Heba H. El-Maghrabi [1], Shaimaa M. Abdelmaged[2], Amr Ahmed Nada[1], Fouad Zahran[3,4], Saad Abd El-Wahab[5], Dena Yahea[5] G. M. Hussein[2], and M. Satrees[2]

## Abstract

Nanocomposites of Ferberite-graphene oxide were prepared via a simple sonication method. The structure, surface morphology and chemical composition were characterized by Fourier-transform infrared spectroscopy (FT-IR), X-ray diffraction (XRD), Raman, energy dispersive X-ray spectrometer (EDS), transmission electron microscopy (TEM), selected area electron diffraction (SAED). XRD results confirm the interaction of Ferberite with graphene oxide. A fast adsorption of the uranium from aqueous solution was observed with an efficiency of 90.6 % within 30 min. the adsorption of uranium ions could be well-described by the Langmuir, Freundlich isotherms and pseudo-second kinetic models.

**Keywords**: Graphene Oxide, Nano-Ferberite, Uranium, Adsorption.

---

[1]Egyptian Petroleum Research Institute, 11727, Cairo, Egypt
[2]Nuclear Materials Authority, 6530 P.O Box Maadi, Cairo, Egypt
[3]Faculty of Science Helwan University, Cairo, Egypt
[4]Institue of Food Science Research (CIAL), Universidad Autonoma de Madrid (CEI UAM+CSIC), 28049 Madrid, Spain
[5]Faculty of Science Ain shams University, Cairo, Egypt

**Military Technical College**
Kobry El-Kobbah,
**Cairo, Egypt**

I.C.E.E.2016

**8th International Conferenc on Chemical & Environmenta Engineering**
19 – 21 April 2016

## l. Introduction

During the last decades, urgent request on environment protection has substantially promoted the development of nanotechnology for synthesis of neoteric adsorption nanometal oxide materials, such as $Fe_2O_3$, $WO_3$ and ZnO, has been including explored to remove of radioactivity and toxicity from contaminated waste water [1, 2]. Uranium, a toxic radioactive element that enters the environment through activities associated with the nuclear industry [1], can cause water contamination, which results in dangerous problems for human health and damage of bio-organisms. For that reason, highly efficient removal of uranium from water is extremely important. Various methods of removing uranium from aqueous solutions, including ion exchange, adsorption, chemical precipitation, membrane processes and solvent extraction [3-16], have been developed. Amongst those techniques, adsorption is extremely significant because of its high efficiency, easy operation, and high concentration factor. A number of absorbents like metal oxides, carbon nanotubes, sepiolites, functionalized clay, chitosan and biosorbents [17- 24] have been investigated for the extraction of uranium from aqueous solutions. However, more than these sorbents have been proved to suffer from the drawback of low sorption capacity.

The significant improvements in nanocomposites performance have been demonstrated by incorporating novel carbonaceous nanomaterials, such as carbon nanotubes (CNTs), graphene and fullerenes [25-30], to form carbon metal nanocomposite. In particular, Graphene, a $sp^2$-bonded carbon sheet with a thickness of single atom as a newly discovered two-dimensional (2-D) carbonaceous material, possesses high electron mobility, high transparency, flexible structure, and large specific surface area, and many researchers have been devoted to studying the several applications of GO or reduced graphene oxide (RGO) as a high performance support or an efficacious adsorbent [31]. In metal oxide–graphene oxide hybrids, GO increasing charge transfer rate of electrons and surface-adsorbed amount of chemical molecules through π–π interactions [32]. Moreover, the formation of M–O–C bonds can expand the pollutant [33, 34]. Thus the integration of nanosized Ferberite with two-dimensional graphene oxide nanosheets offers a great opportunity to design and synthesize Ferberite–graphene hybrid materials with improved adsorption activity.
In this work, we report the preparation of Ferberite–graphene nanocomposites by sonication method, which is used as an effective adsorbent for removal of uranium form waste water.

## 2. Experimental

### 2.1. Materials

Graphite powder (99 wt%), potassium permanganate ($KMnO_4$, 98 wt%), sulfuric acid ($H_2SO_4$, 98 wt%), hydrogen peroxide ($H_2O_2$, 30 wt%), sodium nitrate ($NaNO_3$, 99 wt%), and Ammonium metatungstate hydrate $(NH_4)_6H_2W_{12}O_{40} \cdot xH_2O$ (99%) , iron nitrate $Fe(NO_3)_3 \cdot 9H_2O$ (99%), urea (99%) were purchased from, Fisher chemical, Piochem,

**Military Technical College**
Kobry El-Kobbah,
**Cairo, Egypt**

I.C.E.E.2016

**8th International Conferenc on Chemical & Environmenta Engineering**
19 – 21 April 2016

Scharlow, Adwic , longlive , Adwic , Sigma-aldrich, Merck respectively. All reagents used in this research were superior to chemically pure and used without further purification.

### 2.2. Preparation of ceramic nano-Ferberite:

In the microwave combustion synthesis, Ammonium metatungstate hydrate and iron nitrate were used as precursor; and urea was used as fuel for combustion. Typically, the sol of metal salts with urea mixed in the stoichiometric ratios. The sol was treated in a domestic microwave working at 900 W, 2.45 GHz for 3–5 min [35].

### 2.3. Preparation of graphene oxide (GO)

GO was prepared by oxidizing the graphite powder in a mixture of concentrated sulphuric acid and $KMnO_4$ according to modified Hummers method [36] Fig. (1). Briefly, graphite powder and $NaNO_3$ were stirred in 98% $H_2SO_4$ on a magnetic stirrer for 2 h. Then $KMnO_4$ was gradually added into the above solution by maintaining the temperature less than 20 °C. The mixture was then stirred at 35 °C for 2 h in an oil-bath. The resulting solution was diluted by adding double distilled water under vigorous stirring for 1 h. Then a dark brown suspension was obtained. The suspension was further treated by adding 30 % $H_2O_2$ solution drop wise until the color of the solution became bright yellow. The resulting GO suspension was washed by repeated centrifugation, first with 5 % aqueous HCI solution to remove excess of manganese salt followed by double distilled water until the pH of the solution became near neutral. The purified GO was finally dispersed in double distilled water ultrasonically to obtain a stable dispersion of GO.

### 2.4. Preparation of binary Ferberite –graphene nanocomposites

Magnetic Ferberite -graphene oxide nanocomposite samples were prepared by a simple one-pot. In brief, Ferberite powders were mixed with ultrasonically dispersed GO in aqueous solution for 2 h. The resulting nanocomposite was collected by centrifugation followed by drying at 50 °C for 2 days. After that, the solid was collected. Different content of graphene oxide in FG-x (x: 10, 20 and 30 wt%, respectively) were also obtained to investigate the effect of Ferberite loading. The synthetic route of FGs is shown in Fig. (2).

### 2.5. Characterization

Fourier-transform infrared spectroscopy (FT-IR) spectrum of sample was recorded between 4000 and 500 $cm^{-1}$ with an FTIR spectrometer Perkin Elmer (model spectrum one FT-IR spectrometer, USA). Samples were prepared using the standard KBr pellets. The phase of the powers was identified by an X-ray diffractometer (XRD, Shimadzu XD-l) with a Cu Ka radiation at 40 kV and 30 mA over the 20 range of 4-80° at a scanning speed of 4°/ min with a sampling angle interval of 0.04°. Raman test was carried out using the dispersive Raman microscope (Model Sentera, Bruker, Germany) instrument at laser wave length 532 nm

Military Technical College
Kobry El-Kobbah,
Cairo, Egypt

8th International Conferenc
on
Chemical & Environmenta
Engineering
19 – 21 April 2016

[doubled Nd:YAG laser (neodymium-doped ytrium aluminum garnet)] and power l0 mW . Transmission electron microscopy and Selected area electron diffraction (SAED) was performed on JEOL JEM 2100 were used to characterize the crystallites size and shape of the photocatalysts.

### 2.6. Adsorption experiments

The batch adsorption experiment was carried out in a thermostatic shaker. Blank samples experiment contained deionized water and corresponding prepared nanocomposites are prepared and monitored for the duration of the experiment as a control. The variable parameters on the adsorption process are evaluated under the following conditions:

- Contact time, min 15: 120
- Initial concentration of adsorptive solutions, mg/l 50: 250
- Temperatures, $^{o}$C 25: 70
- PH of solution 1: 10
- Amount of adsorbent, mg 5: 20

For each experimental run, prepared samples $U^{6+}$ solutions of known concentration are transferred into a 50 mL flask, and agitated in a temperature controlled shaker at a constant speed of 200 rpm with a required adsorption time at an ambient temperature and at the required pH.

The concentration of $U^{6+}$ metal ions are determined according to ASTM using UV/Vis spectrophotometer (Jasco V 750, Jaban) equipped.
The adsorption percent and the adsorbed amounts (q) of $U^{6+}$ has been calculated according to the following equations:

$$\text{Adsorption \%} = 100 \times (C_0 - C_t)/ C_0 \quad (1)$$

$$q = (C_0 - C_e)\, V/m \quad (2)$$

**Where** $C_0$ and $C_e$ are the initial and equilibrium concentrations of metal ions (ppm), V is the volume of solution (L), m is the mass of adsorbent (g). All assays were carried out in triplicate and only mean values were presented.

## 3. Results and discussion

### 3.1. Characterization

The XRD patterns of pure GO, pure $FWO_4$ and FGs nanocomposites are shown in Fig. (3) The GO sample prepared by modified Hummers method exhibits two characteristic diffraction peaks at $2\theta$ of 10.8° and 42.5° corresponding to (002) and (100) planes, respectively [37,38]. The (002) diffraction peak corresponds to a larger interlayer distance of approximately 0.82 nm than that of graphite (0.34 nm), implying that the GO sheets are

separated by the covalently bonded oxygen atoms [37, 39, 40].This endows GO with a good hydrophilicity, which is beneficial to an effective dispersion of GO as precursor in aqueous solution [40].

The XRD patterns show that the Ferberite "Tungsten Iron Oxide" prepared is highly crystalline assigned as JCPDS 10-0173, there is no peaks for different phases it confirmed that complete formation of pure Monoclinic Ferberite ($WFeO_4$) phase. Ferberite is a Member of Wolframite Group. The 3D model of Ferberite is observation in Fig. (4) reveals numerous overlapped layers of octahedral structure. The space group is P2/b and the cell parameters are: α = 4.750 Å, b = 5.720 Å, c = 4.970 Å, β = 90°10'. The structure is based on Wand Fe octahedral forming infinite zig-zag chains in the direction of the c axis. Each chain contains just one type of cation and each octahedron is joined to the next by a common edge. Each W-octahedral chain is attached by common corners to four Fe chains, and each Fe chain is also surrounded by four W chains.

The Raman spectroscopy has been often employed for the study of the electronic structure of carbonaceous materials. Fig. (5) Shows the Raman spectra of GO, FWO4 and FGs samples. The typical features of carbonous materials in Raman spectra are G band at 1603 cm-l and D band at 1345 cm-1 [37,41,42]. G band is common for all sp2 carbon forms, due to the in-plane vibration of sp2 bonded carbon atoms, whereas D band is related to the edges, defects and structurally disordered carbons [41, 39].

The Raman spectra for ferberite has no previously been reported. The present results Fig. (5) based on the single-phase of laboratory synthesized ferberite there are three Raman shifts at 215, 281, and 704 cm-1, the first two low wavenumber bands have been assigned to the ν4(Bg) mode, and the 704 cm-1 band to ν3(Bg) and ν3(Eg) virtually pure Wolframite type structures were formed.
In the Raman spectrum of the FGs composites, the two characteristic peaks of G and D bands still exist, showing the virtually reduction of GO through preparation of FGs [43]. Also, an intensity ID<IG of FGs is observed.

The characterization FTIR spectra of the pure GO, pure $FWO_4$ and FGs nanocomposites are demonstrated in Fig. (6). The absorption peak appears around 3600:3400 $cm^{-1}$ is attributed to the O–H stretching vibration and around at 1600:1500 $cm^{-1}$ is attributed to the O–H bending of the surface hydroxyl from adsorbed water, while the absorption at 919, 621 and 477 $cm^{-1}$ is assigned to the Fe–O–W vibration. The FT-IR spectrum of graphene oxide showed the typical skeletal vibration adsorption band of C=C at about 1638 $cm^{-1}$, C–OH at about 1387 $cm^{-1}$, C=O stretching band at about 1742 $cm^{-1}$and C–O stretches at about 1073 $cm^{-1}$ [44, 45], demonstrating the abundant existence of the oxygen-containing functional groups on its surface. Compared to that of the pure $FWO_4$ and FGs samples, bands at 816 and 649 cm-1 correspond to the O-W-O vibration mode and the W-O stretching band, respectively. The absorption band below 1000 $cm^{-1}$ becomes wider for the FGs with increase in ferberite ratio.

**Military Technical College**
Kobry El-Kobbah,
**Cairo, Egypt**

I.C.E.E.2016

**8th International Conferenc on Chemical & Environmenta Engineering**
19 – 21 April 2016

The wider absorption peak can be considered as a combination of Fe–O–W (690 $cm^{-1}$) and W–O–C vibrations (798 $cm^{-1}$) [33], demonstrating the formation of chemical bond between them [34].

The morphologies of the pure GO, pure $FWO_4$ and FGs nanocomposites with different concentrations of ferberite are observed by HR-TEM images. According to Fig. (7). GO displays the crumbled and re-stacked sheet-on-sheet structure with large surface area (about few micrometers in the diameter) which is an advantage for growing ferberite on their surface, the lattice fringe with 0.85 nm (layer spacing), which is assigned to the (101) plane of GO, in which it is distinguish on uniform Ferberite nanoplates through GO layers shape. The nanoparticles of the oxides powder were well synthesized, and had a homogeneous and uniform round grain-shaped structure with a grain size range of 10–15 nm can be clearly seen. The $FWO_4$ can be identified clearly in FG-10 and FG-20 because of the low content of $FWO_4$ (10 and 20 wt% respectively). On the contrary, the excess $FWO_4$ (30 wt%) covered two sides of GO, so no clear GO layers shape were revealed obviously. The semi-quantitative analysis indicates that the weight ratio between Fe and W element in $FWO_4$ nanocomposites as shown in Table (1).

The composition of the $FWO_4$ nanocomposites are determined by energy-dispersive X-ray (EDX) spectroscopy experiment, as is supplied in Fig. (8a). As a result, Fe and W elements were identified, it is possible to form pure stoichiometric $FeWO_4$. Electron diffraction for prepared nano-Ferberite attribute as high poly crystals formation Fig. (8b) confirm with XRD data.

Table 1: The weight ratio composition of the $FWO_4$ and FGs nanocomposites

| Element | Wt % |
|---|---|
| Fe | 48.12 |
| W | 51.88 |

In order to explain the magnetic property of FGs nanocomposites, the magnetic hysteresis curves were measured at room temperature, as demonstrated in Fig. (9). The saturation magnetizations (Ms) of FG-10, FG-20 and FG-30 0.54996, 0.62734 and 0.51235emu/g, respectively. These magnetic properties are quite different from bulk $FeWO_4$ particles (Ms = 4.8287 emu/g Fig. (S1)), but enough for separation [46]. The reduced Ms can be explained by considering the diamagnetic contribution of the GO surrounding the $FeWO_4$, which will weaken the magnetic moment. A simple magnetic recovery system to contrast FGs particles with and without assistant of magnet was also simulated and shown in Fig. (S2). When a magnet approached the dispersion of FG-20, the black nanocomposite were attracted toward the magnet within min and the dispersion became clear seen in Fig. (S2a). However, in Fig. (S2b), the dispersion was not changed obviously after 2 min natural precipitation.

Military Technical College
Kobry El-Kobbah,
Cairo, Egypt

I.C.E.E.2016

8th International Conferenc
on
Chemical & Environmenta
Engineering
19 – 21 April 2016

### 3.2. Adsorption activity

GO, $FWO_4$ and FGs nanocomposites have been chosen as a platform to build new adsorbents for water treatment from radioactivity and toxicity metals ions as U (VI).
The adsorption of U (VI) on FGs was investigated under the conditions of 10 mg adsorbents, 50 mL of U (VI) 100 mg/L solution, initial pH of solution 6.0, and agitated in a temperature controlled shaker at a constant speed of 200 rpm for 2h at an ambient temperature
The adsorption percent of on prepared nanocomposites are illustrated in Fig. (9) removal efficiency on FGs increase with Ferberite content increase from 10 to 30 wt% this may be attributed to that single-layered graphene materials possess two basal planes available for pollutant adsorption. Also Inner sphere complex is formed between the metal ion and electron donating oxygen ions present on FGs surface. Highly adsorption of U (VI) appears on FG-20 nanocomposite with 90 % removal efficiency.

### 3.2.1 Contact time

The effect of contact time was investigated to determine the adsorption equilibrium point for maximum uptake and to establish the kinetics of adsorption process. The adsorption experiments on FG-20 nanocomposite were examined as a function of contact times ranging from 0 to 120 min. The results are shown in Fig. (10). The maximum amounts of adsorption of U (VI) on FG-20 are observed at about 60 min. There is almost no further increase of adsorption after 60 min.

### 3.2.2 Kinetics study

To evaluate the adsorption kinetics of U (VI) ions, pseudo-first-order and pseudo-second-order models were applied to analyze the experimental data [47]. The pseudo-first-order kinetic equation is given as

$$\ln(q_e - q_t) = \ln q_e - k_1 t \qquad (3)$$

**Where** $k_1$ is the rate constant of pseudo-first-order adsorption, $q_e$ and $q_t$ (mg $g^{-1}$) is the amount of uranium adsorbed at equilibrium and at time ($t$), respectively.
The values of $q_e$ and $k_1$ are calculated from the intercepts and slopes of the plot Fig. (11a) corresponding to Eq. (3), which are given in Table (2). The low-related coefficient $R$ and the large difference between the calculated values of adsorption capacity and the experimental values indicate that the sorption mechanism of uranium (VI) on FG does not follow a pseudo-first-order kinetic model well.
The pseudo-second-order adsorption kinetic model is defined as

$$t/q_t = 1/k_2 q_e^2 + t/q_e \qquad (4)$$

Military Technical College
Kobry El-Kobbah,
Cairo, Egypt

8th International Conferenc
on
Chemical & Environmenta
Engineering
19 – 21 April 2016

**Where** $k_2$ is the rate constant of pseudo-second-order adsorption. Fig. (11b) shows straight lines of the pseudo-second-order model with correlation coefficients of 0.9999. Therefore, the adsorption kinetic fits the pseudo-second-order model.

Table (2): Adsorption kinetic parameters

| Metal ions | Adsorbent | $q_{e,exp}$ (mg/g) | Pseudo-first-order kinetics model | | | Pseudo-second-order kinetics model | | |
|---|---|---|---|---|---|---|---|---|
| | | | $q_e$ (mg/g) | $k_1$ ($min^{-1}$) | $R^2$ | $q_e$ (mg/g) | $k_2$ (mg/(g min)) | $R^2$ |
| U(VI) | FG-20 | 455 | 135.6 | -0.011 | 0.580 | 526.2 | 0.0034 | 0.98 |

### 3.2.3 Initial concentration

In the adsorption of U(VI) by FG-20 represented by Fig. (12), the relationship between the quantity of metal ions adsorbed on the adsorbent surface and the concentration remaining in the aqueous phase at equilibrium, can be verified. This relationship showed that the adsorption capacity increases with the equilibrium concentration of U(VI) ions in solution, reaching progressively the adsorbent saturation. The adsorption parameters can be determined by transforming the Langmuir equation to a linear form. Equation 5 represents a better linear regression of the isotherm:

### 3.2.4 Isotherm study

The equilibrium data were analyzed with the help of Langmuir isotherm and Freundlich isotherm models to obtain the best fitting isotherm. These two models are the most common isotherms used to describe the solid–liquid adsorption system.
The Langmuir equation has been used extensively for dilute solutions in the following form

$$C_e/ q_e = 1/bq_m + C_e/q_m \qquad (5)$$

**Where** $C_e$ (mg $L^{-1}$) is the solute equilibrium concentration, $q_e$ (mg $g^{-1}$) is the amount of solution adsorbed per unit mass of the adsorbent, $q_m$ is the maximum adsorption capacity (mg $g^{-1}$), $b$ is Langmuir constant. According to Eq. (5), a straight line is obtained and presented in Fig. (13a). The values of $q_m$ and $b$ are calculated from the slope and the intercept, and are given in Table (3).

The efficiency of the adsorption is expressed in terms of a dimensionless constant separation factor or equilibrium parameter $R_L$, which is defined as follows [48]:

$$R_L = 1/(1+bC_0)$$

**Where** $C_0$ is the initial metal ion concentration. The values of $R_L$ show the isotherm shapes, which are unfavorable ($R_L \geqslant 1$) or favorable ($0 \leqslant R_L \leqslant 1$).
In this study $R_L$ value as 0.0032 indicates that FG-20 is a suitable adsorbent for adsorption of U (VI) from aqueous solutions.

**Military Technical College**
Kobry El-Kobbah,
**Cairo, Egypt**

I.C.E.E.2016

**8th International Conferenc on Chemical & Environmenta Engineering**
19 – 21 April 2016

The Freundlich isotherm can be applied for heterogeneous surfaces and multilayer adsorption, which is expressed as follows [49]:

$$\ln q_e = \ln k + (1/n) \ln C_e \quad (6)$$

**Where** $k$ and $n$ are the Freundlich constants related to the adsorption capacity and adsorption intensity, respectively. They are determined from the intercept and slope of the linear plot of $\ln q_e$ vs. $\ln C_e$ Fig. (13b).

Table (3) Adsorption isotherm parameters

| Metal ions | Adsorbent | Langmuir equation model | | | Freundlich equation model | | |
|---|---|---|---|---|---|---|---|
| | | $q_m$ (mg/g) | $k_L$ | $R^2$ | $k_F$ | n | $R^2$ |
| U(VI) | FG-20 | 525 | 16.6667 | 0.9990 | 255.18 | 4.76 | 0.93 |

### 3.2.5 pH

The adsorption of U (VI) on FG-20 are greatly influenced by the initial pH Fig. (14). the adsorption increases from about 40% to 98% when the pH value increases from 1 to 6, and then rapidly reduces at pH > 6.0.

The surface of adsorbent is positively charged at pH < 4.13. Meanwhile, the dominant U(VI) species is $UO_2^{2+}$ [50], and the electrostatic repulsion between adsorbent and $UO_2^{2+}$ lowers the adsorption ability. As pH value increases, the surface of adsorbent gradually becomes negatively charged. Moreover, functional groups of adsorbent surface become more decentralized. The two variation trends mentioned above increase the adsorption ability between adsorbent and $(UO_2)_3(OH)_5^+$ /$(UO_2)(OH)^+$ , which are the dominant species of U(VI) at pH 4.0 ~ 6.0. When the pH of the aqueous solution is more than 7.0, the surface charge of adsorbent becomes more negative and the main species of U(VI) are $(UO_2)_3(OH)_7^-$ /$(UO_2)(OH)_3^-$. The repulsion between $(UO_2)_3(OH)_7^-$ /$(UO_2)(OH)_3^-$and surface charges results in the drop of adsorption.

### 3.2.6 Adsorbent dosage

The Effect of FG-20 dosage on U (VI) uptake was shown in Fig. (15). U(VI) removal efficiency increased rapidly with the increasing dosage of adsorbent from 0.1 to 0.4 g/L. In this period, with increasing adsorbent dosage more surface area and more active sites were available for adsorption, thus more U(VI) ions could be removed. However, the uptake of U(VI) almost complete (98–100%) as the FG-20 dosage was increased from 15 to 20 mg. Therefore, a dosage of 0.3 g/L was optimal for subsequent adsorption tests.

**Military Technical College**
Kobry El-Kobbah,
**Cairo, Egypt**

**8th International Conferenc on Chemical & Environmenta Engineering**
19 – 21 April 2016

## 4. Conclusion

In summary, nanocomposites of Ferberite–Graphene catalysts (FGs) were prepared from $FWO_4$ and GO by a simple process. The obtained catalysts were characterized by Raman, FT-IR, XRD, EDS and TEM. The influences of $FWO_4$ content were investigated by measuring the adsorption performance for the removal of U (VI). The adsorption efficiency of U (VI) could be obtained 90.5 % at a ferberite content of 20% within 60 min. FGs had relatively higher U(VI) adsorption capacity of 231.1 mg/g at 45 °C than the other known adsorbents, also its could be separated and collected easily from treated solution by an external magnetic field. Moreover, the kinetics of adsorption followed the pseudo second order model, and the equilibrium isotherm studies indicated that Langmuir model could be used to describe the experimental data. Based on the experiments, the interaction between U(VI) and FGs might include electrostatic attraction, chemisorption and physical adsorption. The obtained results indicated that the prepared Ferberite–graphene nanocomposites adsorbents have a potential application for the industrial effluents wastewater treatment containing U (VI) as toxic radioactive element.

## 5. References

[1] E. Craft, A. Abu-Qare, M. Flaherty, M. Garofolo, H. Rincavage and M. Abou-Donia, *J. Toxicol. Environ. Health B Crit. Rev.* 2004, 7, 297-317.
[2] S.C. Sheppard, M. I. Sheppard, M.O. Gallerand and B. Sanipelli, *J. Environ. Radioact.* 2005,79, 55-83.
[3] J.L. Lapka, A. Paulenova, M.Y. Alyapyshev, V.A. Babain, R.S. Herbst and J.D. Law, *Radiochim. Acta*, 2009, 97, 291-296.
[4] D.E. Crean, F.R. Livens, Mustafa Sajih Martin C. Stennett, Daniel Grolimund, C.N. Borcac and N.C. Hyatt, *J. Hazard. Mater.*, 2013, 263, 382-390.
[5] Lucy Mar Camacho, Shuguang Deng and Ramona R. Parra, *J. Hazard. Mater*., 2010, 175, 393-398.
[6] S. B. Xie, C. Zhang, X. H. Zhou, J. Yang, X.J. Zhang and J.S. Wang, *J. Environ. Radioactiv.,* 2009, 100, 162-166.
[7] A. M. Atta, Z. H. Abd El Wahab, Z. A. El Shafey, W. I. Zidan and Z F. Akl, *J. Dispersion Sci. Technol.,* 2010, 31, 1601-1610.
[8] S. Zhang, M. Zeng, J. Li, J. Li, J. Xu and X. Wang, *J. Mater. Chem. A,* 2014, 2, 4391-4397.
[9] A. Gajowiak, M. Majdan and K. Drozdzal*, Przem. Chem*., 2009, 88, 190-196.
[10] I. Zhuravlev, O. Zakutevsky, T. Psareva, V. Kanibolotsky, V. Strelko, M. Taffet and G. Gallios, *J. Radioanal. Nucl. Chem.,* 2002, 254, 85-89.
[11] K. Oshita, M. Oshima, Y.H. Gao, K.H. Lee and S. Motomizu, *Anal. Chim. Acta,* 2003, 480, 239-249.
[12] Y. Zhao, J. Li, S. Zhang, H. Chen and D. Shao, *RSC Adv.*, 2013, 3, 18952-18959.

[13] Y. Liu, Qin Li, X. Cao , Y. Wang, X. Jiang, M. Lee, M. Hua and Z. Zhang, *Appl. Surf. Sci*., 2013, 285, 258-266.
[14] P. Liang, Y.C. Qin, B. Hu, T.Y. Peng and Z.C. Jiang, *Anal. Chim. Acta,* 2001, 440, 207-213.
[15] S. Zhang, J. Li, X. Wang, Y. Huang, M. Zeng and J. Xu, *J. Mater. Chem. A*, 2015, 3, 10119–10126.
[16] S. Zhang, J. Li, X. Wang, Y. Huang, M. Zeng and J. Xu, *J. ACS Appl. Mater. Interfaces,* 2014, 6, 22116-22125.
[17] D.R. Lovley, E.J.P. Phillips, Y.A. Gorby, E.R. Landa, Nature 350 (1991) 413–416.
[18] M.J. Comarmond, T.E. Payne, J.J. Harrison, S. Thiruvoth, H.K. Wong, R.D. Aughterson, G.R. Lumpkin, K. Müller, H. Foerstendorf, Environ. Sci. Technol. 45 (2011) 5536–5542.
[19] J. Wang, P. Liu, Z. Li, W. Qi, Y. Lu and W. Wu, *Materials,* 2013, 6, 4168-4185.
[20] A. Gopalan, M. F. Philips, J. H. Jeong and K. P. Lee, *J.* Nanosci, *Nanotechnol.*, 2014, 14, 2451-2458.
[21] J. N. Dawoud, *Appl. Surf. Sci*., 2012, 259, 433-440.
[22] V. V. Didenko, V.C. Moore, D.S. Baskin and R.E. Smalley, *Nano Letters*, 2005, 5, 1563-1567.
[23] R. B. Mathur, S. Seth, C. Lal, R. Rao, B. P. Singh and T. L. Dhami, *Carbon*, 2007, 45,132-40.
[24] Zhe Wang, H. A. Colorad, Zhan-Hu Guo, Hansang Kim, Cho-Long Park, H. Tomas Hahn, Sang-Gi Lee, Kun-Hong Lee and Yu-Qin, *Mat. Res.*, 2012, 15, 510-516.
[25] B. S. Stankovich, D. A. Dikin, R. D. Piner, K. A. Kohlhaas, A. Kleinhammes, Y. Jia, Yue Wu, S. T. Nguyen and S. Rodney, *Carbon*, 2007, 45, 1558-1565.
[26] Z. Abdeen, *J. Dispersion Sci. Technol.,* 2011, 32, 1337-1344.
[27] C. Ding, W. Cheng, Y. Sun and X. Wang, Dalton Trans., 2014, 43, 3888–3896.
[28] Y. Sun, Q. Wang, C. Chen, X. Tan and X. Wang, Environ. Sci. Technol., 2012, 46, 6020–6027.
[29] Y. Sun, S. Yang, Y. Chen, C. Ding, W. Cheng and X. Wang, Environ. Sci. Technol., 2015, 49, 4255–4262.
[30] Y. Sun, S. Yang, C. Ding, Z. Jin and W. Cheng, RSC Adv., 2015, 5, 24886–24892.
[31] Y. Sun, D. Shao, C. Chen, S. Yang and X. Wang, Environ. Sci. Technol., 2013, 47, 9904–9910.
[32] C. Ding, W. Cheng, Y. Sun and X. Wang, J. Hazard. Mater., 2015, 295, 127–137.
[33] S. Stankovich, D. A. Dikin, G. H. B. Dommett, K. M. Kohlhaas, E. J. Zimney, E. A. Stach, R. D. Piner, S. T. Nguyen and R. S. Ruoff, Nature, 2006, 442, 282–286.
[34] Q. Wang, X. K. Wang, Z. F. Chai and W. P. Hu, Chem. Soc. Rev., 2013, 42, 8821–8834.
[35] Y.P. Peng, S.L. Lo, H.H. Ou, S.W. Lai, J Hazard Mater 183 (2010) 754–758.
[36] Hummers, William S.; Offeman, Richard E., Journal of the American Chemical Society 80. 6 (March 20, 1958) 1339.
[37] W.Q. Fan, Q.H. Lai, Q.H. Zhang, Y. Wang , J Phys Chem. C 115 (2011) 10694–10701.
[38] Q.Q. Zhai, B. Tang, G.X. Hu, J. Hazard. Mater. 198 (2011) 78.

[39] S.D. Perera, R.G. Mariano, N. Nijem, Y. Chabal, J.P. Ferraris, K.J. Balkus Jr, J Power Sources 215 (2012) 1–10.
[40] A.H. Ye, W.Q. Fan, Q.H. Zhang, W.P. Deng, Y. Wang, Catal Sci Technol 2 (2012) 969–978.
[41] P. Cheng, Z. Yang, H. Wang, W. Cheng, M.X. Chen, W.F. Shangguan, Int J Hydrogen Energy 37 (2012) 2224–2230.
[42] O. Akhavan, M. Abdolahad, A. Esfandiar, M. Mohatashamifar, J Phys Chem. C 114 (2010) 12955–12959.
[43] Wang, Y.K. Zhou, B. Xiong, Y.Y. Zhao, X.J. Huang, Z.P. Shao, Electrochim Acta 88 (2013) 847–857.
[44] Q. Feng, K. Liu, J. Fu, Y. Zhang, Z. Zheng, C. Wang, Y. Du, W. Ye, Electrochimica Acta 60 (2012) 304–308.
[45] T.T. Tung, T.Y. Kim, J.P. Shim, W.S. Yang, H. Kim, K.S. Suh, Organic Electronics 12 (2011) 2215–2224.
[46] D.D. Shao, C.L. Chen, X.K. Wang, Chem. Eng. J. 185–186 (2012) 144–150.
[47] Y. S. Ho and G. McKay, 1999., 34(5): 451– 465.
[48] A. Bhatnagar, A.K. Jain, J. Colloid Interface Sci., 28 (2005), pp. 49–55
[49] Freundlich, Uber die adsorption in losungen, Z. Phys. Chem. 57 (1906) 385–470.
[50] Songnan Li, Hongbin Bai, Jun Wang, Xiaoyan Jing, Qi Liu, Milin Zhang, Rongrong Chen, Lianhe Liu, Caishan Jiao, Chemical Engineering Journal 193–194 (2012) 372–380

Military Technical College
Kobry El-Kobbah,
Cairo, Egypt

I.C.E.E.2016

8th International Conferenc
on
Chemical & Environmenta
Engineering
19 – 21 April 2016

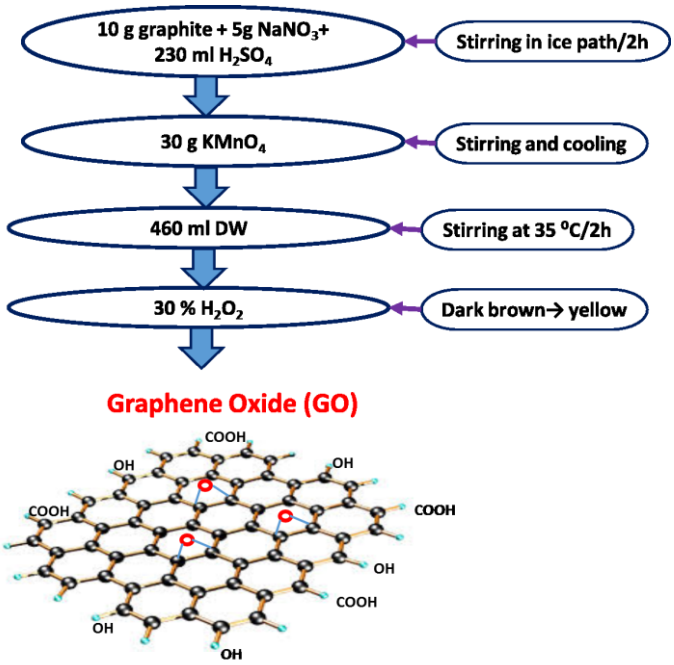


**Fig. (1): Schematic diagram for synthesis of GO.**

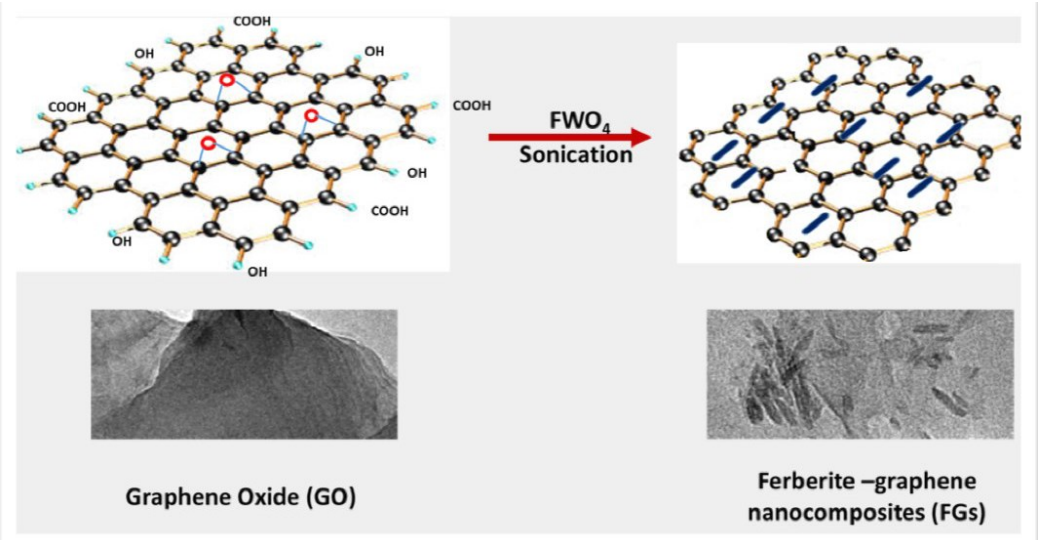


**Fig. (2): The synthetic route of FGs**

Military Technical College
Kobry El-Kobbah,
Cairo, Egypt

I.C.E.E.2016

8th International Conferenc
on
Chemical & Environmenta
Engineering
19 – 21 April 2016

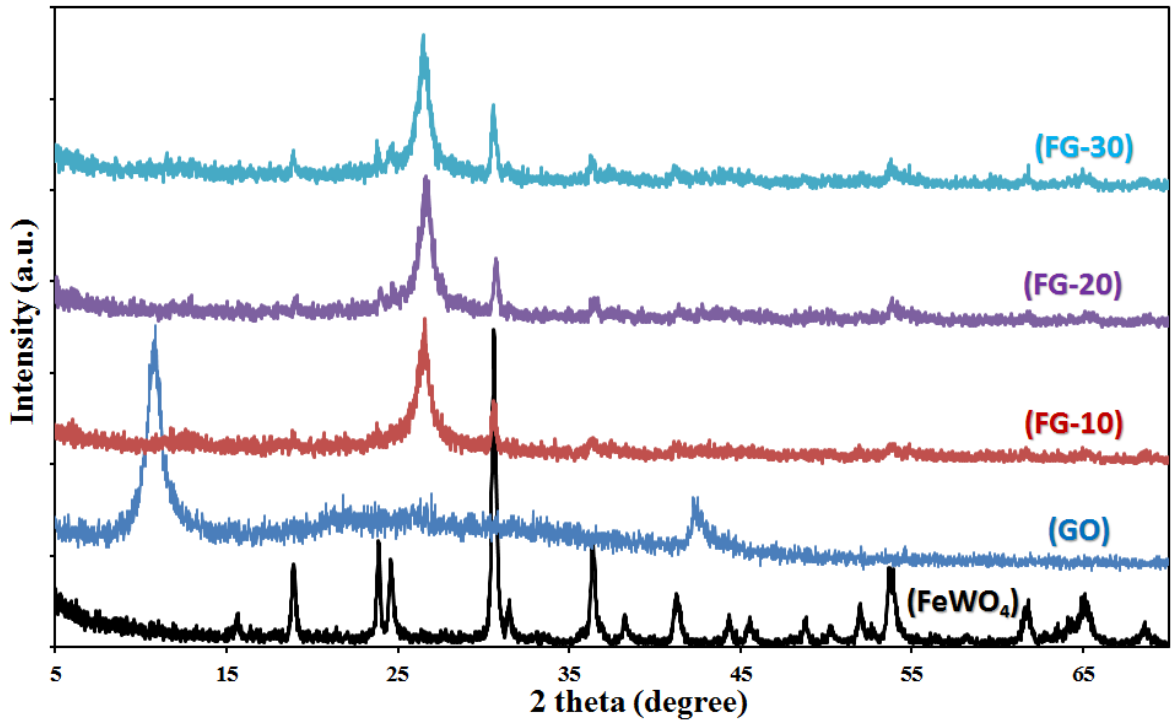


**Fig. (3): XRD patterns of $FeWO_4$, GO and FGs nanocomposites.**

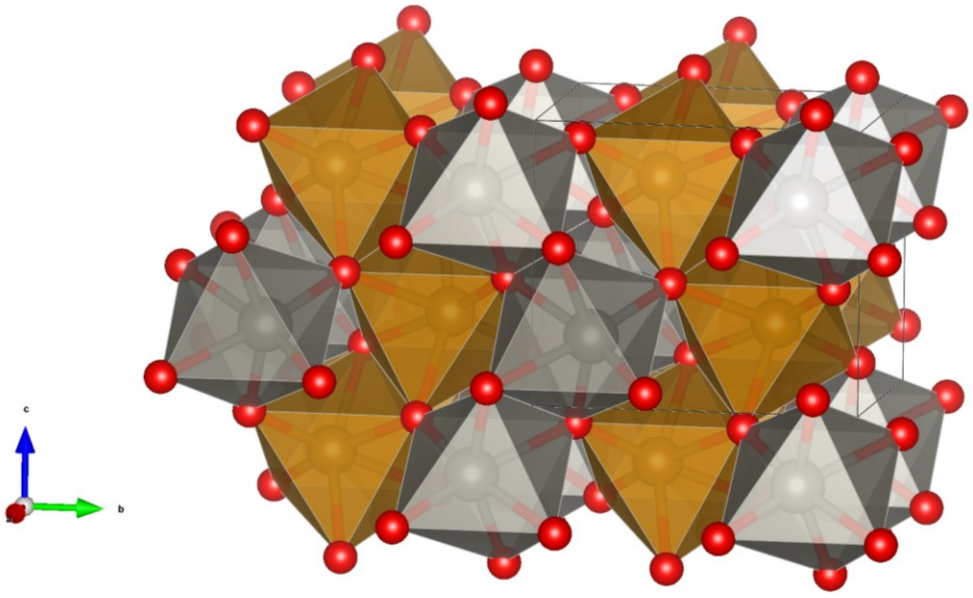

Fe – red-orange, W – grey, O – red

**Fig. (4): The crystal structure of Ferberite ceramics.**

Military Technical College
Kobry El-Kobbah,
Cairo, Egypt

I.C.E.E.2016

8th International Conferenc
on
Chemical & Environmenta
Engineering
19 – 21 April 2016

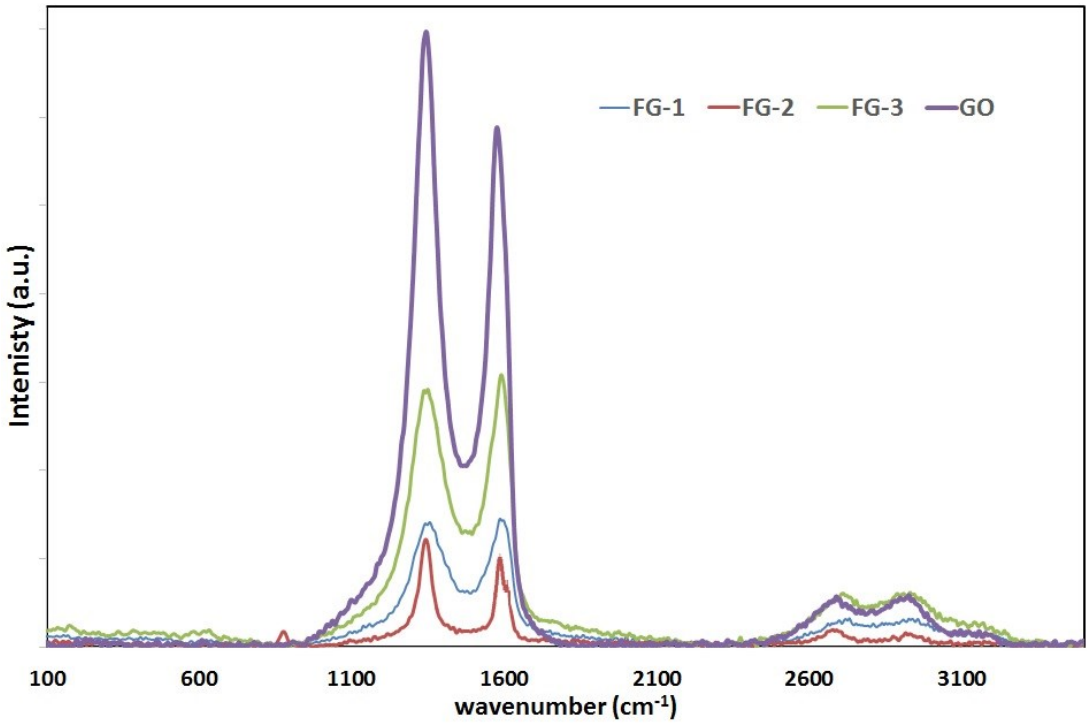


**Fig. (5): Raman spectra of GO, $FWO_4$ and FGs nanocomposites.**

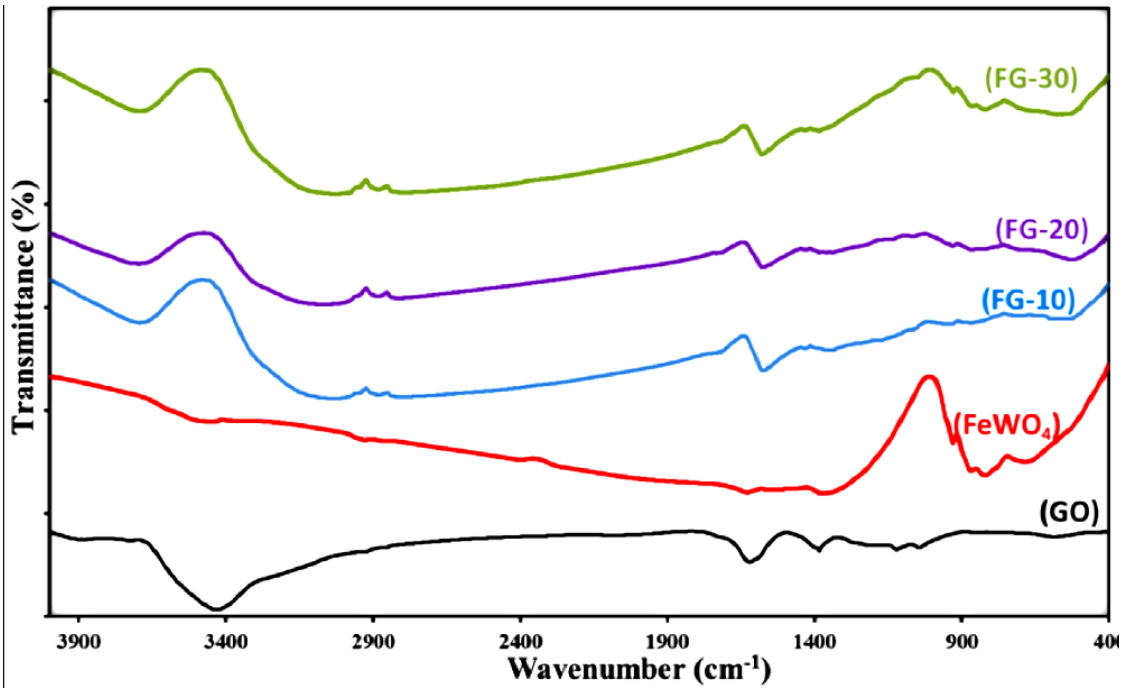


**Fig. (6): FTIR curves of GO, $FWO_4$ and FGs nanocomposites.**

**Military Technical College**
Kobry El-Kobbah,
**Cairo, Egypt**

I.C.E.E.2016

**8th International Conferenc**
**on**
**Chemical & Environmenta**
**Engineering**
19 – 21 April 2016

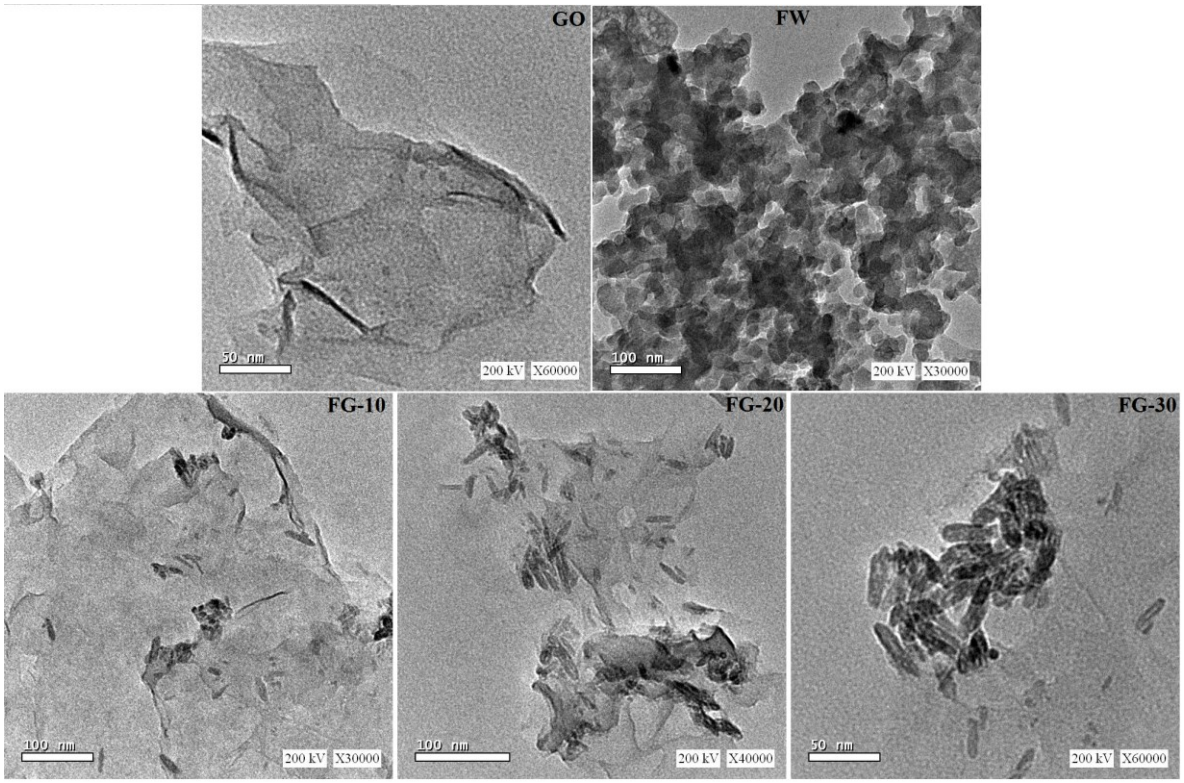


**Fig. (7): HR-TEM images of GO, FW and FGs nanocomposites.**

Military Technical College
Kobry El-Kobbah,
Cairo, Egypt

I.C.E.E.2016

8th International Conferenc
on
Chemical & Environmenta
Engineering
19 – 21 April 2016

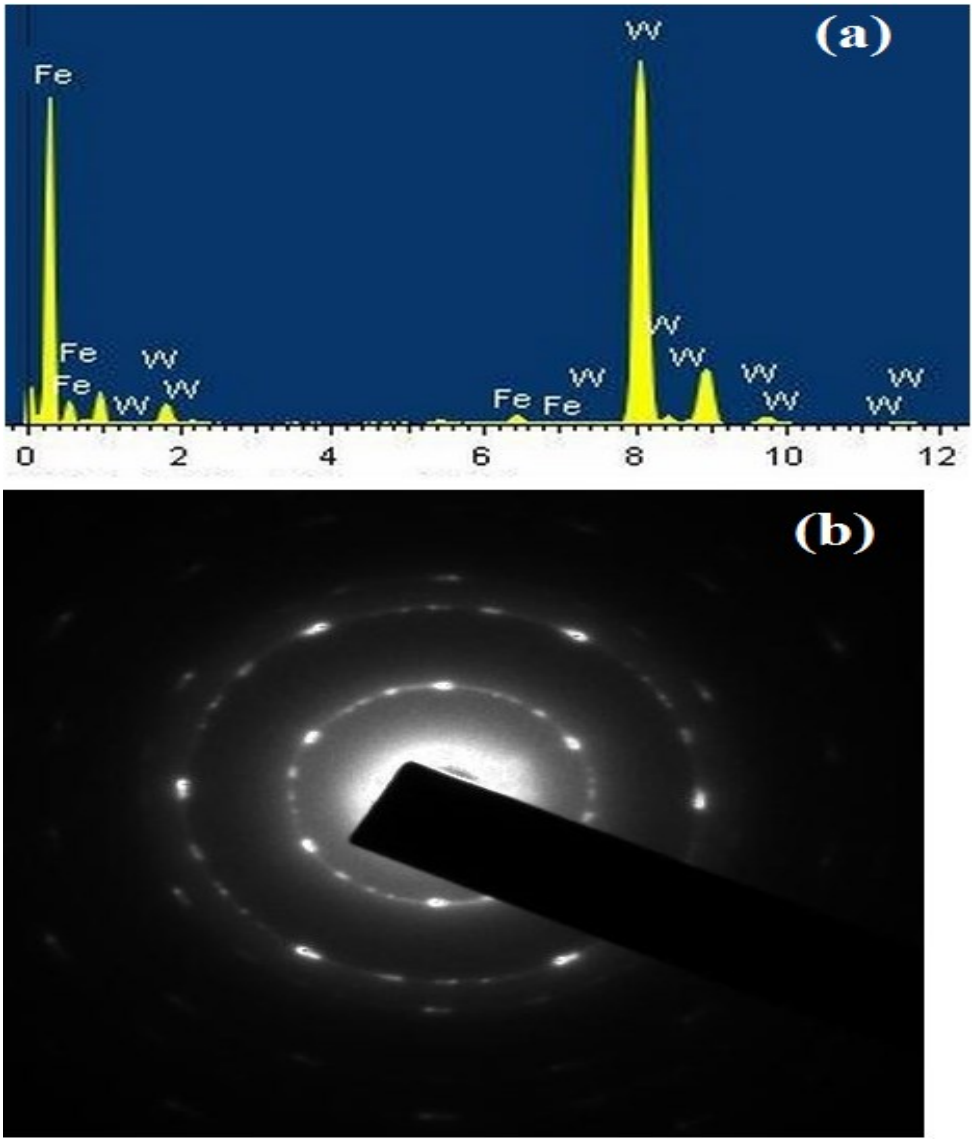


**Fig. (8): The energy-dispersive X-ray (EDX) and Electron diffraction of the $FWO_4$ nanocomposites.**

Military Technical College
Kobry El-Kobbah,
Cairo, Egypt

I.C.E.E.2016

8th International Conferenc
on
Chemical & Environmenta
Engineering
19 – 21 April 2016

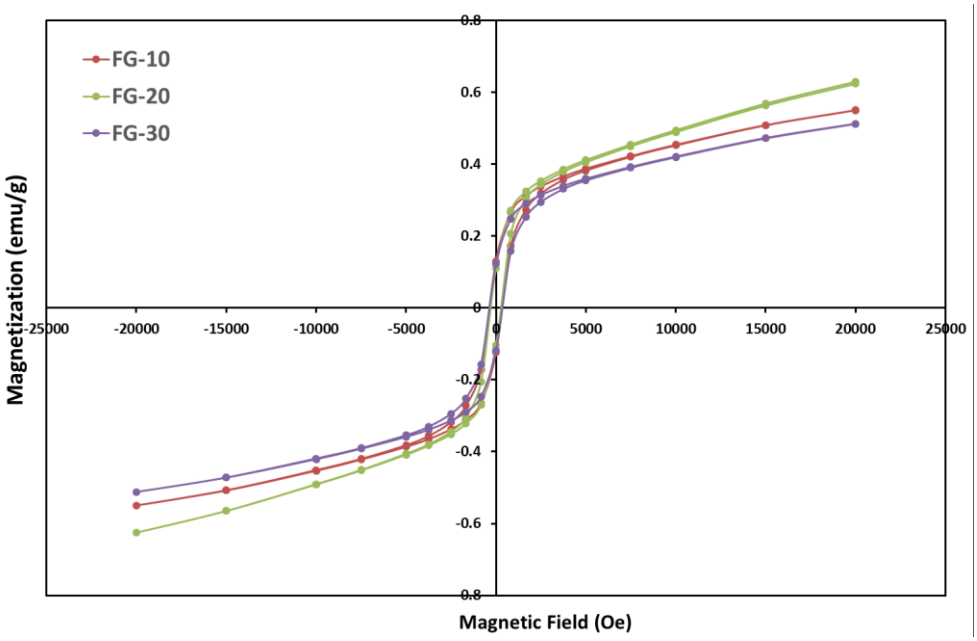


**Fig. (8): The Magnetization curves of FGs nanocomposites.**

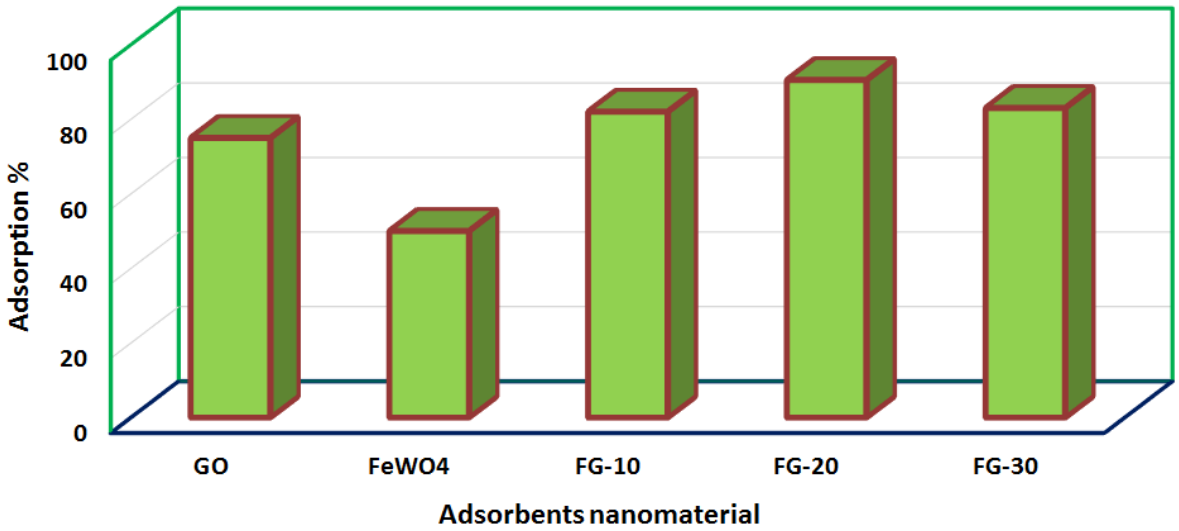


**Fig. (9) The adsorption efficiency of UVI.**

Military Technical College
Kobry El-Kobbah,
Cairo, Egypt

I.C.E.E.2016

8th International Conferenc
on
Chemical & Environmenta
Engineering
19 – 21 April 2016

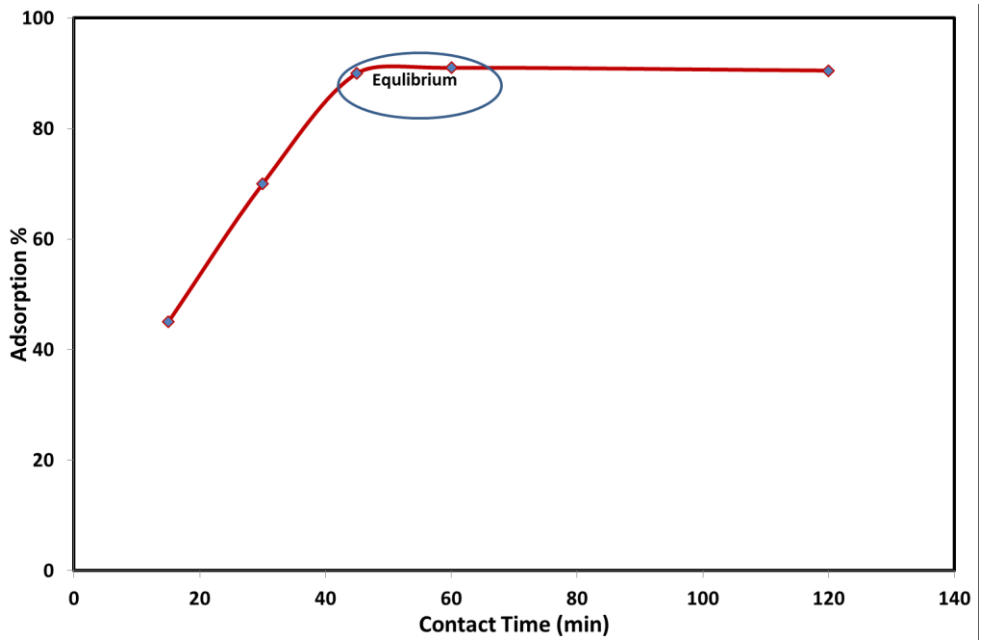


**Fig. (10): Effect of contact time on adsorption of uranium**

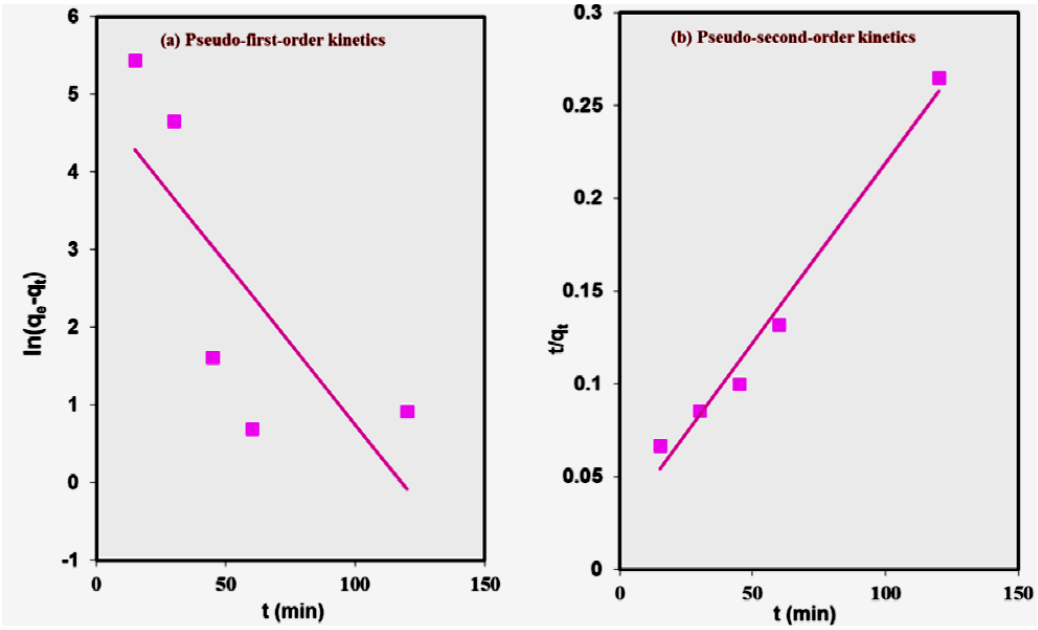


**Fig. (11): The adsorption kinetics**

Military Technical College
Kobry El-Kobbah,
Cairo, Egypt

I.C.E.E.2016

8th International Conferenc
on
Chemical & Environmenta
Engineering
19 – 21 April 2016

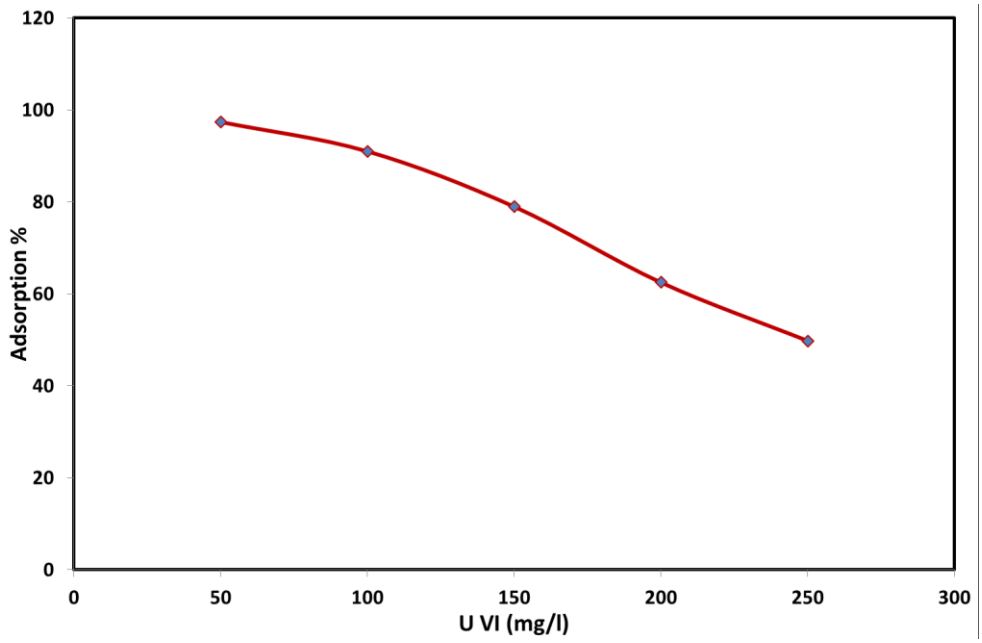


**Fig. (12): Effect of Initial U(VI) concentration on the adsorption.**

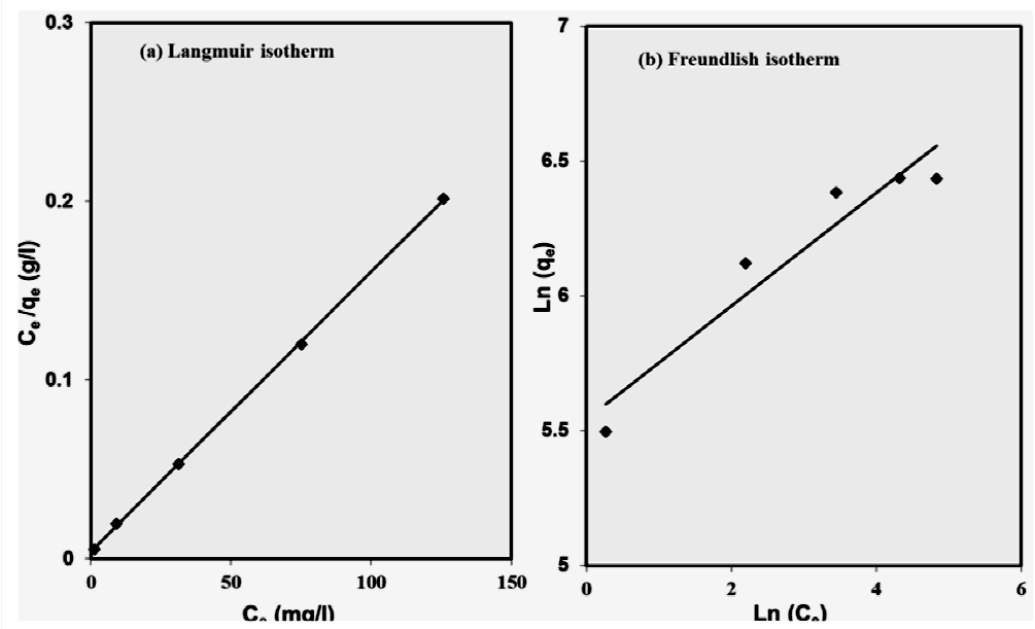


**Fig. (13): Langmuir and Freundlich isotherm models**

Military Technical College
Kobry El-Kobbah,
Cairo, Egypt

I.C.E.E.2016

8th International Conferenc
on
Chemical & Environmenta
Engineering
19 – 21 April 2016

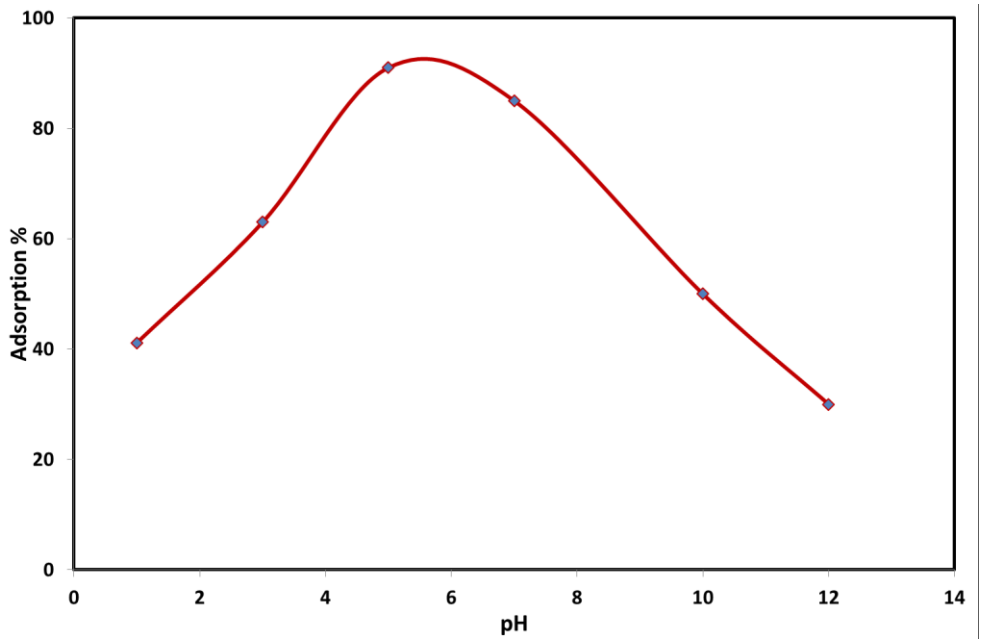


**Fig. (14): Effect of pH on adsorption of uranium**

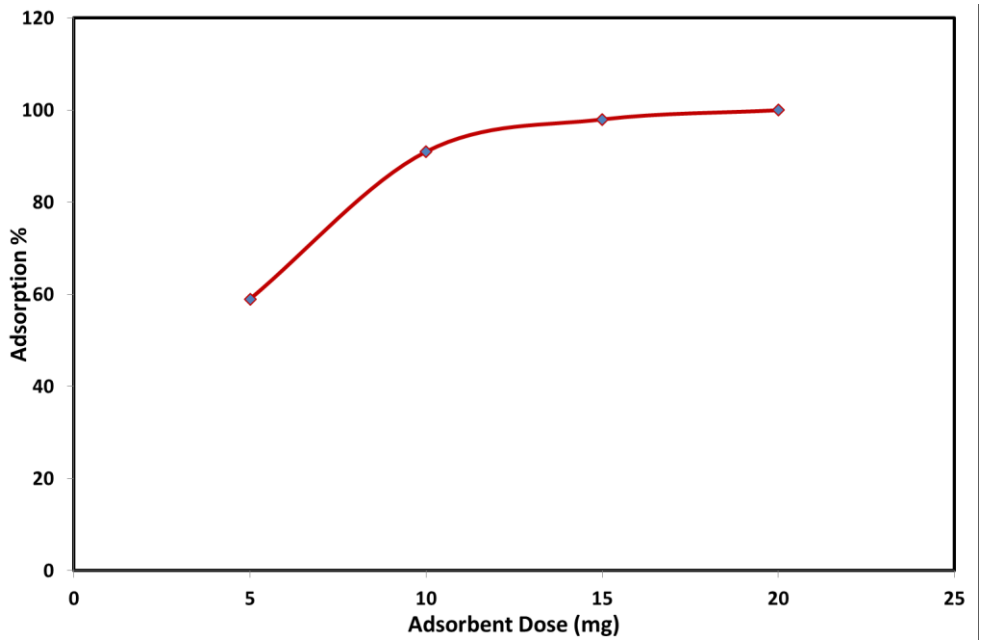


**Fig. (15): Effect of Adsorbent dosage on adsorption of uranium**